J. Plasma Phys. (2020), *vol*. 86, 905860516
Published by Cambridge University Press
doi:10.1017/S002237782000118X

Compton scattering in particle-in-cell codes

F. Del Gaudio [1],†, **T. Grismayer** [1],†, **R. A. Fonseca** [1,2] **and L. O. Silva** [1],†

[1]GoLP/Instituto de Plasmas e Fusão Nuclear, Instituto Superior Técnico, Universidade de Lisboa, 1049-001 Lisbon, Portugal

[2]DCTI/ISCTE Instituto Universitário de Lisboa, 1649-026 Lisboa, Portugal

(Received 25 June 2020; revised 27 August 2020; accepted 2 September 2020)

We present a Monte Carlo collisional scheme that models single Compton scattering between leptons and photons in particle-in-cell codes. The numerical implementation of Compton scattering can deal with macro-particles of different weights and conserves momentum and energy in each collision. Our scheme is validated through two benchmarks for which exact analytical solutions exist: the inverse Compton spectra produced by an electron scattering with an isotropic photon gas and the photon–electron gas equilibrium described by the Kompaneets equation. It provides new opportunities for numerical investigation of plasma phenomena where a significant population of high-energy photons is present in the system.

Key words: plasma simulation, astrophysical plasmas, quantum plasma

1. Introduction

Computer simulations for kinetic plasma processes are of core interest for a variety of scenarios, ranging from astrophysics to laboratory experiments. The particle-in-cell (PIC) methodology (Evans & Harlow 1957; Dawson 1983; Hockney & Eastwood 1988; Bird 1989; Birdsall & Langdon 1991) is one of the most popular and widely used techniques, which pioneered the study of collisionless plasmas. The standard PIC loop can be enriched with various quantum electrodynamics (QED) cross sections to investigate astrophysical environments and model laboratory experiments where quantum processes affect the plasma dynamics. These modules rely on Monte Carlo techniques by taking advantage of the inherent stochasticity of QED processes. The coupling of QED Monte Carlo modules to the PIC loop represents a unique numerical tool that allows such scenarios to be studied from first principles. For example, the inclusion of nonlinear Compton scattering (QED synchrotron) is essential to simulate the interaction of matter with ultra-intense electromagnetic fields (Nerush *et al.* 2011; Ridgers *et al.* 2012; Blackburn *et al.* 2014; Vranic *et al.* 2014; Gonoskov *et al.* 2015; Grismayer *et al.* 2016; Jirka *et al.* 2016; Lobet *et al.* 2016; Vranic *et al.* 2016*a*,*b*; Grismayer *et al.* 2017). Several other radiative energy loss channels can participate in the production of high-energy photons, such as curvature radiation, inverse Compton emission, and Bremsstrahlung. These photons are produced in astronomical sources such as active galactic nuclei, X-ray binaries, supernova remnants,

† Email addresses for correspondence: fabrizio.gaudio@tecnico.ulisboa.pt, thomas.grismayer@ist.utl.pt, luis.silva@ist.utl.pt

pulsars and gamma-ray bursts can further interact with matter and, in particular, with the surrounding plasma. The wavelengths of high-energy photons are typically smaller than the average inter-particle distance of any tenuous plasma, implying only binary interaction between single photons and electrons. The leading photon–electron (positron) interaction mechanism is single Compton scattering (Compton 1923).

The collision of high-energy photons with the plasma electrons is at the core of some fundamental scenarios: explains the saturation properties of cyclotron radiation masers (Dreicer 1964), the relaxation to the thermal equilibrium of a photon–electron gas (Kompaneets 1957; Peyraud 1968*a*,*b*,*c*), or the Comptonisation of the microwave background (Sunyaev & Zel'dovich 1980). These seminal studies approximate the plasma as a gas of free electrons and, thus, neglect its collective behaviour. Frederiksen, Haugbølle & Nordlund (2008) and, more recently, the present authors (Del Gaudio *et al.* 2020) have shown that bursts of hard X-rays can couple to the collective plasma dynamics via incoherent Compton scattering events and drive plasma wakes. Such phenomena can be studied numerically by coupling a Monte Carlo Compton module to the PIC loop (Haugbølle 2005; Haugbølle, Frederiksen & Nordlund 2013), in a binary collision module.

The implementation of binary collisions in PIC codes is discussed extensively in the literature, with the main focus on Coulomb collisions (Takizuka & Abe 1977; Wilson, Horwitz & Lin 1992; Miller & Combi 1994; Vahedi & Surendra 1995; Nanbu 1997; Larson 2003; Kawamura & Birdsall 2005; Sentoku & Kemp 2008; Sherlock 2008; Peano *et al.* 2009; Turrell, Sherlock & Rose 2015; Higginson 2017). The usual implementation relies on the approximation of small cumulative scattering angles (Takizuka & Abe 1977; Miller & Combi 1994; Nanbu 1997), which allows the simulation time step that is not bound to resolve the collision frequency to be relaxed. Recently, Turrell *et al.* (2015) and Higginson (2017) included the effect of large angle deflections in Coulomb collision algorithms. The definition of a cut-off angle allows the occurrence of small-angle collisions or large-angle collisions to be identified, based on the impact parameter of the colliding particles. Coulomb collisions differ from Compton collisions in kinematics. In electron–ion collisions, the recoil on the massive ion can usually be neglected. Instead, in photon–electron collisions the electron recoil cannot be neglected unless in the Thomson limit. Notably, Goudsmit & Saunderson (1940) have developed a electron multiple scattering theory in the case of elastic collisions, which can be applied to the Thomson regime. To the best of the authors' knowledge, a multiple scattering theory for Compton scattering has not yet been developed. Thus, we employ a single scattering procedure where the collision frequency has to be properly resolved by the time discretisation. In general, the smallness of the cross section would result in single scattering events per simulation time step. For particularly high photon densities, the time resolution must be imposed by the collision routine rather than the usual Courant condition for the field solver.

In this article, we describe the implementation of a single Compton scattering collision module for PIC codes. It relies on first principles that the Klein–Nishina (Klein & Nishina 1923) cross section is employed with no approximations and allows a self-consistent treatment of the high-frequency radiation coupling with the plasma dynamics. In § 2, we review the basic theory for Compton scattering with particular attention paid to the Lorentz invariant quantities that the model must enforce for reproducing the correct scattering rates in the collision at relativistic energies (Peano *et al.* 2009). Section 3 is devoted to the implementation of our collision procedure. In § 4, we benchmark our code against problems for which exact analytical solution or formulation exist, namely the scattering photon spectrum of a relativistic charge (Blumenthal & Gould 1970), and the Kompaneets equation (Kompaneets 1957). Finally, in § 5, we comment on the computational cost that

https://doi.org/10.1017/S002237782000118X Published online by Cambridge University Press

our module brings as compared with a standard PIC loop. Summary and conclusions are presented in § 6.

2. Compton scattering

Single Compton scattering is the inelastic collision between a photon and an electron (Compton 1923). It is the generalisation of Thomson scattering (Thomson 1906), for any value of the incident photon of energy $\hbar\omega$ in the electron proper frame of reference. By applying energy and momentum conservation in the electron rest frame, later denoted reference frame (O),

$$\hbar\omega + mc^2 = \hbar\omega' + \gamma' mc^2, \tag{2.1}$$

$$\hbar\boldsymbol{k} = \hbar\boldsymbol{k}' + \boldsymbol{p}', \tag{2.2}$$

where $\gamma' = \sqrt{1 + p'^2/m^2c^2}$ and $\omega = ck$, the photon frequency shift over one collision is

$$\frac{\omega'}{\omega} = \frac{mc^2}{mc^2 + \hbar\omega(1 - \cos\theta)}, \tag{2.3}$$

where ω (ω') is the absorbed (emitted) frequency, and θ is the scattering angle. For $\hbar\omega \ll mc^2$, the Thomson limit $\omega' \simeq \omega$ is recovered. However, when the incident photon energy approaches and exceeds the electron rest mass energy $\hbar\omega \gtrsim mc^2$, the energy transfer becomes relevant. For $\hbar\omega \gg mc^2$, at $\theta \simeq -\pi$, the photon transfers up to half its energy $\hbar(\omega - \omega') \simeq \hbar\omega/2$ to the electron. The classical theory of radiation explains Thomson scattering in terms of plane wave absorption and consequent dipole radiation from the oscillating charge (Landau & Lifshitz 1975; Jackson 1999), but does not predict Compton scattering, which is intrinsically a quantum process.

2.1. *Klein–Nishina cross section*

In the rest frame of an electron, the single Compton scattering probability is determined by the Klein–Nishina differential (in solid angle Ω) cross section (Klein & Nishina 1923), which, for unpolarised photons, reads

$$\frac{\mathrm{d}\sigma}{\mathrm{d}\Omega} = \frac{r_e^2}{2}\left(\frac{\omega'}{\omega}\right)^2\left(\frac{\omega'}{\omega} + \frac{\omega}{\omega'} - \sin^2\theta\right), \tag{2.4}$$

where $r_e = e^2/mc^2$ is the classical electron radius. By combining (2.3) and (2.4), and integrating over the solid angle $\mathrm{d}\Omega = \sin\theta\,\mathrm{d}\theta\,\mathrm{d}\phi$ (ϕ is the symmetry angle around the direction of the incoming photon) the total cross section reads

$$\sigma(\epsilon) = \frac{\pi r_e^2}{\epsilon}\left[\left(1 - \frac{2}{\epsilon} - \frac{2}{\epsilon^2}\right)\log(1 + 2\epsilon) + \frac{1}{2} + \frac{4}{\epsilon} - \frac{1}{2(1 + 2\epsilon)^2}\right], \tag{2.5}$$

where $\epsilon = \hbar\omega/mc^2$. In the limit for low photon energies

$$\lim_{\epsilon \to 0}\sigma(\epsilon) = \sigma_T \tag{2.6}$$

the Thomson cross section is recovered. For high photon energies $\epsilon \gg 1$, the cross section has the limiting expression

$$\lim_{\epsilon \gg 1}\sigma(\epsilon) = \frac{3}{8}\sigma_T\frac{\log(2\epsilon)}{\epsilon} \tag{2.7}$$

and decreases with respect to the incident photon energy.

https://doi.org/10.1017/S002237782000118X Published online by Cambridge University Press

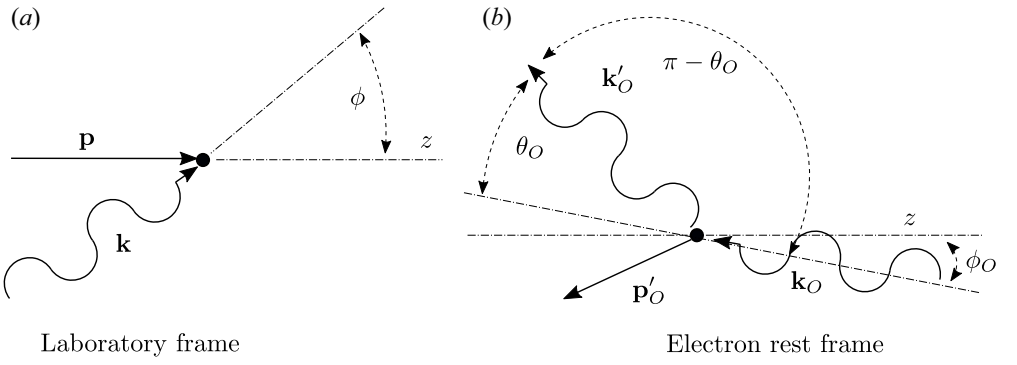

FIGURE 1. Schematic of the Compton scattering relativistic kinematics.

2.2. *Relativistic kinematics and Lorentz invariants*

We consider a relativistic electron which propagates along the z coordinate at velocity βc and scatters with a photon at an incident angle ϕ in the laboratory frame, see figure 1. In the electron proper frame of reference $_O$, the incident angle is modified by relativistic effects. In the frame $_O$ the incident photon is confined within a small cone (Blumenthal & Gould 1970)

$$\tan\phi_O = \frac{\sin\phi}{\gamma(\cos\phi - \beta)} \tag{2.8}$$

of aperture $1/\gamma$. The photon energy in the frame $_O$ reads

$$\epsilon_O = \gamma\epsilon(1 - \beta\cos\phi). \tag{2.9}$$

It varies in the range $\epsilon_O \in [\epsilon/2\gamma, 2\gamma\epsilon]$ according to the incident angle ϕ. In the $_O$ frame, the photon energy after scattering obeys (2.3) and in the laboratory frame reads

$$\epsilon' = \gamma\epsilon'_O[1 + \beta\cos(\pi - \theta_O - \phi_O)] \simeq \gamma\epsilon'_O(1 - \cos\theta_O), \tag{2.10}$$

owing to the Lorentz transformation, where $\beta \simeq 1$ and $\phi_O \sim 1/\gamma$. In the Thomson regime, $\omega'_O \simeq \omega_O$ and the maximum energy achieved over one collision is $\epsilon' \simeq 4\gamma^2\epsilon$, for $\phi \simeq \pi$ and $\theta_O \simeq \pi$. In the extreme Klein–Nishina limit, the maximum energy achieved over one collision can be obtained by combining (2.3), (2.9), and (2.10), and reads $\epsilon' \simeq \gamma$.

We now consider the scattering between photons, with distribution function f_ω, and electrons, with distribution function f_e. Within a portion of space-time $\mathrm{d}\boldsymbol{x}\,\mathrm{d}t$, the number of collisions is a Lorentz invariant quantity (Groot, Leeuwen & van Weert 1980) that is given by

$$N = \sigma(\boldsymbol{p}, \boldsymbol{k})cf_\omega\,\mathrm{d}\boldsymbol{k}f_e\,\mathrm{d}\boldsymbol{p}\,\mathrm{d}\boldsymbol{x}\mathrm{d}t. \tag{2.11}$$

In general, the cross section $\sigma(\boldsymbol{p}, \boldsymbol{k})$ depends on the electron momentum $\boldsymbol{p}$, and on the photon wavevector $\boldsymbol{k}$. As the space-time element $\mathrm{d}\boldsymbol{x}\,\mathrm{d}t$, the distribution functions f_ω and f_e, and the speed of light c are Lorentz invariant, therefore $\sigma(\boldsymbol{p}, \boldsymbol{k})\,\mathrm{d}\boldsymbol{k}\,\mathrm{d}\boldsymbol{p}$ is also Lorentz invariant (Landau & Lifshitz 1975). This invariance allows us to obtain the cross section in any inertial frame ($\gamma = \sqrt{1 + \boldsymbol{p}^2/m^2c^4}$, $\epsilon = \hbar|\boldsymbol{k}|/mc$). Knowing the cross section in the

https://doi.org/10.1017/S002237782000118X Published online by Cambridge University Press

electron proper frame of reference ($\gamma_O = 1, \epsilon_O = \gamma\epsilon - \hbar \boldsymbol{p}\cdot\boldsymbol{k}/m^2c^2$)

$$\sigma(\boldsymbol{p},\boldsymbol{k})\,\mathrm{d}\boldsymbol{k}\,\mathrm{d}\boldsymbol{p} = \sigma(\omega_O)\,\mathrm{d}\boldsymbol{k}_O\,\mathrm{d}\boldsymbol{p}_O, \tag{2.12}$$

we finally obtain

$$\sigma(\boldsymbol{p},\boldsymbol{k}) = \sigma(\epsilon_O)\frac{\epsilon_O}{\gamma\epsilon}, \tag{2.13}$$

because $\mathrm{d}\boldsymbol{k}/\epsilon$ and $\mathrm{d}\boldsymbol{p}/\gamma$ are Lorentz invariants (Landau & Lifshitz 1975).

3. Single Compton scattering algorithm

The implementation of single Compton scattering in a PIC code must not only recover the correct microphysics of the process (frequency shift, angle, momentum recoil) but must preserve the invariant number of collisions to obtain the correct scattering rates (Peano *et al.* 2009). The implementation follows naturally as each macro-particle represents an ensemble of real particles that are close neighbours in phase space. Each macro-particle has a weight q that relates to the number of real particles it represents and, thus, samples a portion of the distribution function of real particles. Figure 2 outlines our implementation that follows three steps: (i) binning of the macro-particles into collision cells $\Delta\boldsymbol{x}$, a volume in configuration space, (ii) pairing of the colliding macro-particles according to their probability $P^{i,j}$ of interaction within $\Delta\boldsymbol{x}\Delta t$, (iii) update of the momenta of the scattering macro-particles.

3.1. *Macro-particles binning*

The binning of macro-particles in collision cells naturally uses the single PIC cell as the smallest binning volume. The size of a PIC cell is also the smallest scale over which the self-consistent plasma collective fields are computed. For this reason, the collision cells are usually set equal to the PIC cells. Macro-photons and macro-electrons are binned in the collision cells and sorted such that we identify the indexes of macro-electrons and macro-photons within each collision cell.

3.2. *Pairing*

For each collision cell, we pair the scattering couples and add them to a scattering list using the no-time-counter (NTC) method (Bird 1989; Abe 1993). The NTC method is a popular Monte Carlo scheme for collision procedures involving single scattering events (not for cumulative scattering). The standard pairing routines for cumulative Coulomb collisions allow for a time step larger than the collision frequency, thus all macro-particles are involved in the scattering process each time step. Instead, the NTC method applies when the time step resolves the collision frequency such that the maximum possible number of macro-scatterings within a time step involves only a subset of all the macro-particles. Developed three decades ago (Bird 1989), NTC provides a cost reduction for the sampling of a discrete probability distribution function. We detail now the NTC algorithm applied to single Compton scattering.

We consider a collision cell containing N_ω macro-photons and N_e macro-electrons. A conservative upper-bound to the maximum probability of any macro-particle to collide within Δt is

$$P_{\max} = 2\sigma_T c\Delta t \max[q_e^i, q_\omega^j], \tag{3.1}$$

where $\max[q_e^i, q_\omega^j]$ is the largest weight with units of a density among all macro-particles in the collision cell ($i \in [1, N_e]$ macro-electrons and $j \in [1, N_\omega]$ macro-photons). The factor 2 appears conservatively as the upper bound in the relativistic transformation of the cross

https://doi.org/10.1017/S002237782000118X Published online by Cambridge University Press

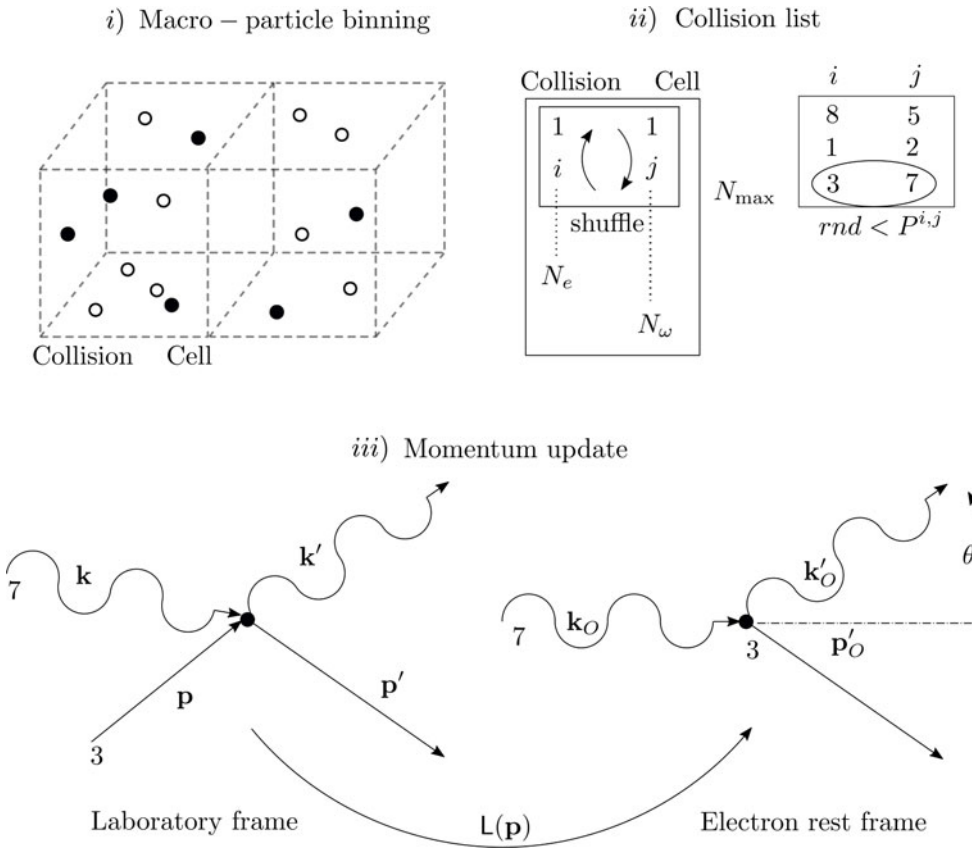

FIGURE 2. Schematic of the Compton scattering algorithm. It follows three steps: (i) the macro-particles are binned into collision cells $\Delta \boldsymbol{x}$, (ii) the probability $P^{i,j}$ of interaction within $\Delta \boldsymbol{x} \Delta t$ is computed and scattering macro-particles are chosen using the no-time-counter method, (iii) the momenta of the scattering macro-particles are updated.

section $\sigma = \sigma_{T,O}\epsilon_O/\gamma\epsilon$, where $\max(\epsilon_O) = 2\gamma\epsilon$. The maximum number of macro-particles that can scatter $N_{\max}$ is given by the maximum probability $P_{\max}$ times the number of all the possible unsorted pairing combinations $N_e N_\omega$ (potential scatterings) of the macro-photons with the macro-electrons. It reads

$$N_{\max} = P_{\max} N_e N_\omega. \tag{3.2}$$

The number $N_{\max}$ is usually not an integer and is rounded to the next or previous integer by a Monte Carlo sampling of the residue. This procedure preserves statistically the correct number of collisions within $\Delta \boldsymbol{x} \Delta t$. We randomly pair $N_{\max}$ macro-photons and $N_{\max}$ macro-electrons. This follows two steps: (i) the random sorting of the macro-photons and the macro-electrons, (ii) the selection of the first $N_{\max}$ indexes. At this point, we have a shortlist of $N_{\max}$ randomly paired macro-particles, which contains the maximum possible scatterings in the collision cell. For each pair in the short list, a random number $\mathrm{rnd} \in [0, 1]$ is rolled and compared with the joint probability

$$P^{i,j} = \sigma(\boldsymbol{p}^i, \boldsymbol{k}^j) c \Delta t \max[q_e^i, q_\omega^j]/P_{\max} \tag{3.3}$$

of scattering after having being selected within the $N_{\max}$ pairs.

https://doi.org/10.1017/S002237782000118X Published online by Cambridge University Press

To compute the cross section $\sigma(\boldsymbol{p}^i, \boldsymbol{k}^j)$ we proceed as follows. The energy of the photon $\boldsymbol{k}^j$ is Lorentz boosted in the rest frame of the electron $\boldsymbol{p}^i$

$$\epsilon_O^j = \gamma^i \epsilon^j - \hbar \boldsymbol{p}^i \cdot \boldsymbol{k}^j / m^2 c^2. \tag{3.4}$$

Then, the cross section $\sigma_C(\epsilon_O^j)$ is computed in this frame and boosted back into the simulation frame using (2.13). A macro-electron/macro-photon pair from the shortlist is admitted to the scattering list based on a rejection method (accepted if rnd $< P^{i,j}$).

3.3. *Momentum update*

For each pair in the scattering list, the momenta are updated according to the Compton frequency shift and momentum recoil. The macro-photon four-wavevector $\mathcal{K} = (\epsilon, \hbar \boldsymbol{k}/mc)$ is Lorentz boosted in the rest frame of the electron, of momentum $\boldsymbol{p}$ in the simulation frame, as $\mathcal{K}_O = \boldsymbol{L}(\boldsymbol{p})\mathcal{K}$, where the boost matrix is

$$\boldsymbol{L}(\boldsymbol{p}) = \begin{bmatrix} \gamma & -\boldsymbol{p}/mc \\ -\boldsymbol{p}^T/mc & \boldsymbol{I} + \boldsymbol{p}^T\boldsymbol{p}/m^2c^2(1+\gamma) \end{bmatrix}, \tag{3.5}$$

and $\boldsymbol{I}$ the 3×3 identity matrix. In the frame O, we identify the unit vector along the photon propagation direction $\hat{\boldsymbol{k}}_0$, which defines the symmetry axis for the scattering. We define an orthonormal unit vector base $\hat{\boldsymbol{e}}_1 = \hat{\boldsymbol{k}}_0$, $\hat{\boldsymbol{e}}_2 \perp \hat{\boldsymbol{e}}_1$, $\hat{\boldsymbol{e}}_3 = \hat{\boldsymbol{e}}_1 \times \hat{\boldsymbol{e}}_2$. The two scattering angles θ and ϕ are then sampled, θ is the angle with respect to $\hat{\boldsymbol{e}}_1$ and ϕ is the angle on the plane $\hat{\boldsymbol{e}}_2, \hat{\boldsymbol{e}}_3$. This latter parameter, being the angle of rotational symmetry, is chosen randomly between 0 and 2π. The angle θ, or rather the parameter $\mu = \cos\theta$, is obtained by the inverse transform sampling method of the cumulative probability function given by the differential cross section of the process (see appendix A). We preferred this method rather than a rejection method, whose efficiency decreases for $\epsilon_O \gtrsim 1$ owing to the steepening of the probability density function close to $\mu \simeq -1$. The scattered photon energy is ϵ'_O given by (2.3)

$$\epsilon'_O = \frac{\epsilon_O}{1 + \epsilon_O(1-\mu)} \tag{3.6}$$

and the scattered wavevector is

$$\frac{\hbar \boldsymbol{k}'_O}{mc} = \epsilon'_O \left(\mu \hat{\boldsymbol{e}}_1 + \sqrt{1-\mu^2}\cos\phi \hat{\boldsymbol{e}}_2 + \sqrt{1-\mu^2}\sin\phi \hat{\boldsymbol{e}}_3 \right). \tag{3.7}$$

We transform back to the simulation frame $\mathcal{K}'_O = (\epsilon'_O, \hbar \boldsymbol{k}'_O/mc)$ simply as $\mathcal{K}' = \boldsymbol{L}(-\boldsymbol{p})\mathcal{K}'_O$, and by conservation of momentum the scattered electron has a new momentum $\boldsymbol{p}' = \boldsymbol{p} + \hbar(\boldsymbol{k} - \boldsymbol{k}')$.

3.4. *Macro-particles with difference in weight*

In PIC codes, it is unlikely that two scattering particles possess the same weight. Two main techniques to approach the problem have been discussed in Sentoku & Kemp (2008). The first approach is based on a rejection method for which the scattering occurs with a probability based on the weights of the two-scattering macro-particles. This method does not reproduce the energy and momentum transfer of each collision but only on average, for a sufficiently high number of macro-particles in the collision cell. To preserve the energy and momentum transfer per collision, an alternative is first to spilt the scattering macro-particle of weight q into a scattering fraction q_s ($\boldsymbol{p}_s$) and a non-scattering

https://doi.org/10.1017/S002237782000118X Published online by Cambridge University Press

fraction $q_{\rm ns}$ ($\boldsymbol{p}$). After the collision takes place, the two fractions are merged again into the macro-particle q, which has the average energy and momentum of q_s and $q_{\rm ns}$. This last method becomes inaccurate when $\boldsymbol{p}_s$ differs significantly from $\boldsymbol{p}$ such that the two fractions q_s and $q_{\rm ns}$ refer to two well-distinct portions of the phase space. This issue has already been addressed by Haugbølle (2005) and relies on splitting and merging at two different steps. Here, we address this problem similarly but only the largest weight macro-particle is split before scattering. We briefly recall the main steps of the splitting procedure:

(i) identify the two scattering macro-particles of weight q_e^i and q_ω^j, and select the largest weight between the two $\max[q_e^i, q_\omega^j]$;
(ii) create a new particle of weight equal to $\min[q_e^i, q_\omega^j]$;
(iii) the two macro-particles of equal weight $\min[q_e^i, q_\omega^j]$ are now paired and can be Compton scattered as described previously; and
(iv) reassign to the split macro-particle the weight $\max[q_e^i, q_\omega^j] - \min[q_e^i, q_\omega^j]$.

The splitting is performed within the scattering routine and can lead to a significant increase of macro-particles in the simulation. Merging algorithms (Vranic *et al.* 2015) can be used at a different step of the PIC loop to preserve the number of macro-particles in the simulation within a reasonable maximum, thus avoiding their exponential increase. The advantage of merging at a later stage is that only macro-particles close in phase space merge. Details can be found in Vranic *et al.* (2015). Here we have not used the merging algorithm, but it can be straightforwardly combined with the algorithm described here.

4. Benchmarks

To benchmark our algorithm, we choose two problems that possess an exact analytical solution:

(i) the inverse Compton spectra produced by an electron scattering with an isotropic photon gas (Blumenthal & Gould 1970); and
(ii) the relaxation to the thermal equilibrium of a photon gas by Compton collisions with a thermal electron gas of fixed non-relativistic temperature described by the Kompaneets equation (Kompaneets 1957).

4.1. *Inverse Compton spectra*

Blumenthal & Gould (1970) derived the inverse Compton spectra produced by the collision of a relativistic electron, $\gamma \gg 1$, with an isotropic gas of photons (see appendix B). The scattered photon distribution function reads

$$f(\Gamma, \mathcal{E}') = 2q\log q + (1+2q)(1-q) + \frac{1}{2}\frac{\Gamma^2 q^2}{1+\Gamma q}(1-q), \tag{4.1}$$

where $q = \mathcal{E}'/[1+\Gamma(1-\mathcal{E}')]$, $\mathcal{E}' = \epsilon'/\epsilon'_{\rm max}$ is the scattered photon energy normalised to its maximum $\epsilon'_{\rm max} = \gamma\Gamma/(1+\Gamma)$. The parameter $\Gamma = 4\epsilon\gamma$ relates to the energy of the scattering photons in the electron rest frame and distinguishes two regimes: (i) Thomson limit $\Gamma \ll 1$ and (ii) extreme Klein–Nishina limit $\Gamma \gg 1$.

Figure 3 shows the excellent agreement between our simulations (dashed lines) and theory (4.1) (solid lines) for $\Gamma = 0.1, 10, 100$. The scattered photon distribution function $f(\Gamma, \mathcal{E}')$ is normalised $\int \mathrm{d}\mathcal{E}' f(\Gamma, \mathcal{E}') = 1$. In our simulations, the photon gas is initialised with 1.5×10^7 macro-photons, which mimic an emission line. All macro-photons have the same energy and are propagating in random directions, distributed uniformly on the surface of a sphere in momentum space. We considered the interaction at different photon

https://doi.org/10.1017/S002237782000118X Published online by Cambridge University Press

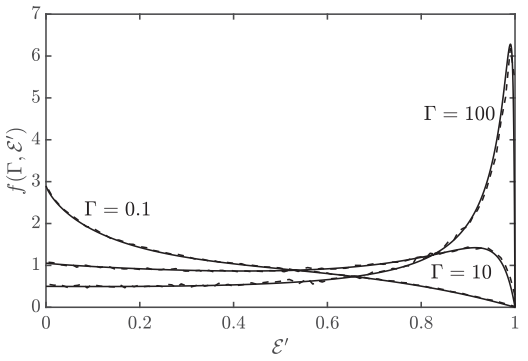

FIGURE 3. Scattered photon distribution function $f(\Gamma, \mathcal{E}')$ for $\Gamma = 0.1, 10, 100$. The simulation results are shown by dashed lines and the theory (4.1) by solid lines (Blumenthal & Gould 1970).

energies $\epsilon = 0.00025, 0.025, 0.25$. An equal number of macro-electrons is initialised at a Lorentz factor of $\gamma = 100$, all collimated in one direction. To avoid that, each macro-photon scatters more than once the simulation runs for only a single time step where about 1×10^6 macro-scatterings occur. The only constraint on Δt is to be low enough such that $P_{\max} < 1$, to prevent multiple collisions of the photons to occur within a single time step.

4.2. *Photon–electron gas equilibrium (Kompaneets equation)*

Kompaneets addressed the thermodynamic equilibrium established between photons and free electrons if their interaction is only mediated by Compton scattering events (Kompaneets 1957). Kompaneets derived the partial differential equation that describes the temporal evolution of the photon occupation number n resulting from the interaction with an electron gas of fixed non-relativistic temperature $k_B T \ll mc^2$, where k_B is the Boltzmann constant. The full collision operator reads

$$\frac{\partial n}{\partial t} = c \int \mathrm{d}\boldsymbol{p} \frac{\mathrm{d}\sigma}{\mathrm{d}\Omega} \left[f_e' n' (1 + n) - f_e n (1 + n') \right], \tag{4.2}$$

where $f_e = f_e(\gamma)$ and $f_e' = f_e(\gamma')$ refer to the electron energy distribution function evaluated at a Compton transition $\gamma mc^2 + \hbar\omega \rightleftharpoons \gamma' mc^2 + \hbar\omega'$. The evaluation of the photon occupation numbers $n = n(\omega)$ and $n' = n(\omega')$ follow the same definition. The n^2 terms account for the photon Bose–Einstein statistics when phenomena such as stimulated scattering and superposition of states are considered. The full Boltzmann operator can be reduced to a Fokker–Planck form within the Thomson limit $\hbar\omega \ll mc^2$ (see appendix C). In regimes where the photon occupation number is small, $n \ll 1$, the photon electron gas interaction is mediated by single Compton scattering events and the linear Kompaneets equation in terms of the photon energy distribution function $f = \xi^2 n$ reads

$$\frac{\partial f}{\partial y} = \frac{\partial}{\partial \xi} \left[\xi^2 \frac{\partial f}{\partial \xi} + \left(\xi^2 - 2\xi \right) f \right], \tag{4.3}$$

where $y = t/t_C$, $t_C = mc/\sigma_T n_e k_B T$ is the characteristic relaxation time and $\xi = \hbar\omega/k_B T$ is the photon energy normalised to the electron temperature.

Figure 4 shows the excellent agreement between our algorithm and the numerical solution of the linear Kompaneets equation (4.3) obtained with a finite-difference

https://doi.org/10.1017/S002237782000118X Published online by Cambridge University Press

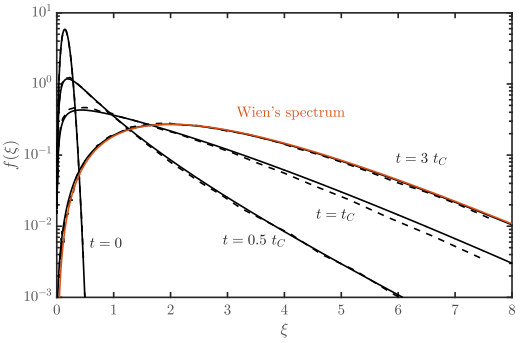

FIGURE 4. Time evolution of the photon distribution function $f(\xi)$ by the interaction with an electron gas of density 10^{18} cm^{-3} at 5 keV temperature for times $t = 0, 0.5, 1, 3\ t_C$. After $t = 3\ t_C$ the photon distribution function resembles the Wien spectrum and does not evolve significantly. Simulations in dashed lines and solution of the linear Kompaneets equation (4.3) in solid lines (Kompaneets 1957).

centred scheme. In our simulation, more than 10^5 macro-photons are initialised to mimic an emission line at an average energy of $\bar{\xi} = \langle \xi \rangle = 0.2$. The emission line has a small energy spread of $\sigma_\xi^2 = \langle \xi^2 - \bar{\xi}^2 \rangle = 0.1$, and the initial distribution

$$f(\xi, y = 0) \propto \exp\left[-\frac{\left(\xi - \bar{\xi}\right)^2}{2\sigma_\xi^2} \right] \tag{4.4}$$

is Maxwellian. The same number of macro-electrons is sampled according to a Maxwellian distribution at a temperature of $k_B T = 5$ keV. To enforce a constant electron temperature during the simulation for a rigorous comparison with theory, we turn off the Lorentz force, which will arise from fluctuations in the electron density. We also omit the momentum, and energy ceded by the electron to the photons at each collision such that the electron population does not cool down. At $t \gtrsim 3\ t_C$, the photon energy distribution reaches equilibrium and converges towards the Wien's spectrum $f \propto \xi^2 \exp(-\xi)$, the correct equilibrium for the linear Kompaneets equation, as expected from the underlying hypothesis.

5. Considerations on the algorithm performance

In this section, we compare the computational cost of our Compton scattering algorithm with the standard PIC loop. The computational performance of our algorithm is usually dependent on the physical parameters of the particular simulated system. A thorough benchmark of its performance should then cover a variety of physical parameters of relevant case scenarios. In collisional plasmas, a typical benchmark of the performance of a collisional algorithm relies on the simulation of thermal plasma with and without collisions. Our choice for the comparison follows a similar criterion. We simulate in one dimension a thermal plasma in equilibrium with a photon gas, both at a temperature of 5 keV. The plasma density is $n_p = 10^{18}$ cm^{-3} and the photon density is $n_\omega = 3 \times 10^{27}$ cm^{-3}, chosen such that the electron Compton collision frequency is a tenth of the plasma frequency $c\sigma_T n_\omega = \omega_p/10$. The electrons follow a Maxwell–Boltzmann distribution $f \propto \sqrt{W_k} \exp(-W_k/k_B T)$, and the photons follow a Wien distribution $f \propto W_k^2 \exp(-W_k/k_B T)$. The computational domain is divided into 240 cells. The time step is $\Delta t = 0.099\ \omega_p^{-1}$. Periodic boundary conditions are used. Figure 5 shows the time of

https://doi.org/10.1017/S002237782000118X Published online by Cambridge University Press

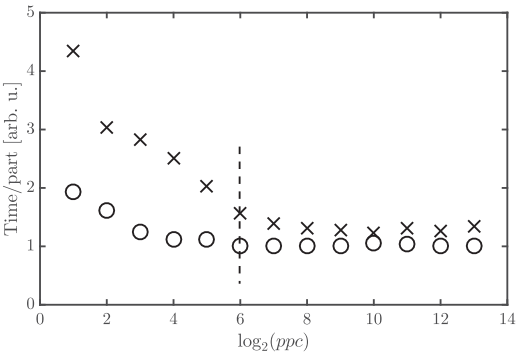

FIGURE 5. Time of a PIC loop per simulation particle with (×) and without (○) Compton collisions as a function of the number of particles per cell (ppc). For a low number of ppc, the loop time is determined by the particle sorting routine (dependent also on the number of grid cells) used by the Compton module. For a sufficiently high number of ppc, the scaling of our collision algorithm is proportional to the amount of simulated particles.

a PIC loop per simulation particle with (×) and without (○) Compton collisions as a function of the initial number of particles per cell (ppc). In this comparison macro-particle splitting occurs, but not particle merging. For a low number of ppc, the loop time is determined by the particle sorting routine (dependent also on the number of grid cells) used by the Compton module. For a high number of ppc, the scaling of our collision algorithm is proportional to the number of simulated particles. The computational cost of the sorting routine scales with both the number of simulated macro-particles and the number of cells in which they are sorted. Therefore, there is a trade-off, which for the set of parameters of these simulations occurs around 64 ppc and is highlighted by the dashed line in figure 5. Beyond the region delimited by the dashed line (which changed depending on the grid size and the number of ppc), the inclusion of the Compton algorithm does not affect significantly the standard PIC loop performance. This trade-off must be assessed for the different numerical parameters/configurations to determine the optimal performance conditions.

6. Summary

We have presented a collision algorithm that incorporates the effect of single Compton scattering from high-frequency photons in PIC codes. This allows a self-consistent treatment of the high-frequency radiation coupling with the plasma dynamics from first principles. The algorithm shows excellent agreement with respect to the benchmarks: scattering photon spectrum from the collision with relativistic electrons (Blumenthal & Gould 1970) and the relaxation to thermal equilibrium of a photon population with an electron gas (Kompaneets 1957). This framework is at the forefront for the numerical modelling of photon–plasma interaction and opens new and exciting opportunities in the numerical investigation of plasma phenomena where a significant population of hard photons is present in the system.

Acknowledgements

This work was supported by the European Research Council (ERC-2015-AdG grant no. 695088), FCT (Portugal) grants SFRH/IF/01780/2013 and PD/BD/114323/2016 in the framework of the Advanced Program in Plasma Science and Engineering (APPLAuSE,

FCT grant no. PD/00505/2012). Simulations were performed at IST cluster (Portugal) and at MareNostrum (Spain) under a PRACE award.

Editor Antoine C. Bret thanks the referees for their advice in evaluating this article.

Declaration of interests

The authors report no conflict of interest.

Appendix A. Scattering angle by the Inverse Transform Sampling method

The probability distribution function (pdf) of the scattered macro-photon over the scattering angle $\mu = \cos\theta \in [1, -1]$ reads

$$\mathrm{pdf}(\mu, \epsilon_O) = \frac{1}{\sigma(\epsilon_O)}\frac{\mathrm{d}\sigma}{\mathrm{d}\mu}, \quad \text{and} \quad \int_1^{-1} \mathrm{d}\mu \frac{\mathrm{d}\sigma}{\mathrm{d}\mu} = \sigma(\epsilon_O) \tag{A 1a,b}$$

with

$$\frac{\mathrm{d}\sigma}{\mathrm{d}\mu} = -\pi r_e^2 \left(\frac{1}{1+\epsilon_O(1-\mu)}\right)^2 \left(\frac{1}{1+\epsilon_O(1-\mu)} + \epsilon_O(1-\mu) + \mu^2\right). \tag{A 2}$$

The cumulative distribution function (cdf) is

$$\mathrm{cdf}(\mu, \epsilon_O) = \frac{1}{\sigma(\epsilon_O)} \int_1^{\mu} \mathrm{d}\mu' \frac{\mathrm{d}\sigma}{\mathrm{d}\mu'} \tag{A 3}$$

with

$$\int_1^{\mu} \mathrm{d}\mu' \frac{\mathrm{d}\sigma}{\mathrm{d}\mu'} = \frac{\pi r_e^2}{\epsilon_O}\left\{\left(1 - \frac{2}{\epsilon_0} - \frac{2}{\epsilon_0^2}\right)\log\left[1+\epsilon_O(1-\mu)\right] + \frac{1-\mu}{\epsilon_O}\left[1 + \frac{1+2\epsilon_O}{1+\epsilon_O(1-\mu)}\right] + \frac{1}{2} - \frac{1}{[1+\epsilon_O(1-\mu)]^2}\right\} \tag{A 4}$$

In the inverse transform sampling method a random number is generated in the range $\mathrm{rnd} \in [0, 1]$, then $\mu = \mathrm{cdf}^{-1}(\mathrm{rnd}, \epsilon_O)$. Given the nonlinear dependence of the cdf on μ, we use the bisection method to solve $\mathrm{cdf}(\mu, \epsilon_O) - \mathrm{rnd} = 0$.

Appendix B. Photon spectrum: single scattering with a relativistic electron

We briefly recall the main steps in the derivation of (4.1), see Blumenthal & Gould (1970). If the photon gas is isotropic in the laboratory frame, it appears beamed at a small angle $\sim 1/\gamma$ in the proper frame $_O$ of reference of an incident relativistic electron $\gamma \gg 1$, as shown by (2.8). The Compton scattering differential rate in the laboratory frame reads

$$\frac{\mathrm{d}N_\omega}{\mathrm{d}t\,\mathrm{d}\epsilon'} = \int \mathrm{d}\epsilon_O \int \mathrm{d}\Omega_O \frac{\mathrm{d}N}{\mathrm{d}t_O\,\mathrm{d}\epsilon_O\,\mathrm{d}\Omega_O\,\mathrm{d}\epsilon'_O}\frac{\mathrm{d}t_O}{\mathrm{d}t}\frac{\mathrm{d}\epsilon'_O}{\mathrm{d}\epsilon'}. \tag{B 1}$$

The time interval in the frame $_O$ is $\mathrm{d}t_O = \mathrm{d}t/\gamma$, and the energy transforms according to (2.10) as $\mathrm{d}\epsilon' \simeq \gamma(1-\cos\theta_O)\,\mathrm{d}\epsilon'_O$. The Compton scattering differential rate in the frame $_O$ is

$$\frac{\mathrm{d}N}{\mathrm{d}t_O\,\mathrm{d}\epsilon_O\,\mathrm{d}\Omega_O\,\mathrm{d}\epsilon'_O} = c\frac{\mathrm{d}\sigma(\epsilon_O)}{\mathrm{d}\Omega_O}\delta(\epsilon'_O - \epsilon_O)\frac{\mathrm{d}n_O}{\mathrm{d}\epsilon_O}. \tag{B 2}$$

Here $\mathrm{d}\sigma(\epsilon_O)/\mathrm{d}\Omega_O$ is the Klein–Nishina cross section. The photon density spectrum $\mathrm{d}n_O/\mathrm{d}\epsilon_O$ in the $_O$ frame can be related with the isotropic differential photon density in

https://doi.org/10.1017/S002237782000118X Published online by Cambridge University Press

the laboratory frame by the Lorentz invariance of the ratio $\mathrm{d}n/\epsilon$:

$$\frac{1}{\epsilon_O}\frac{\mathrm{d}n_O}{\mathrm{d}\epsilon_O} = \frac{1}{\epsilon}\frac{\mathrm{d}n}{\mathrm{d}\epsilon}. \tag{B 3}$$

The isotropic differential photon density in the laboratory frame reads $\mathrm{d}n = n(\epsilon)\mathrm{d}\cos\phi/2$, where $n(\epsilon)$ is the density of photons of a given energy ϵ. According to (2.9), the incident angle in the laboratory frame results in a change in the photon energy in the $_O$ frame as $|\mathrm{d}\epsilon_O/\mathrm{d}\cos\phi| \simeq \gamma\epsilon$. One thus obtain from (B 3)

$$\frac{\mathrm{d}n_O}{\mathrm{d}\epsilon_O} = \frac{\epsilon_O}{2\gamma\epsilon^2}n(\epsilon). \tag{B 4}$$

By combining (B 4) and (B 2) with (B 1), the Compton scattering differential rate reads (Blumenthal & Gould 1970)

$$\frac{\mathrm{d}N}{\mathrm{d}t\,\mathrm{d}\mathcal{E}'} = \frac{3\sigma_T c}{4\gamma}\frac{n(\epsilon)}{\epsilon}f(\Gamma,\mathcal{E}'), \tag{B 5}$$

where$\mathcal{E}' = \epsilon'/\epsilon'_{\max}$ is the scattered photon energy normalised to its maximum $\epsilon'_{\max} = \gamma\Gamma/(1+\Gamma)$. The parameter $\Gamma = 4\epsilon\gamma$ relates to the energy of the scattering photons in the electron rest frame and distinguishes two regimes: (i) Thomson limit $\Gamma \ll 1$ and (ii) extreme Klein–Nishina limit $\Gamma \gg 1$. The scattered photon distribution function reads

$$f(\Gamma,\mathcal{E}') = 2q\log q + (1+2q)(1-q) + \frac{1}{2}\frac{\Gamma^2 q^2}{1+\Gamma q}(1-q), \tag{B 6}$$

where $q = \mathcal{E}'/[1+\Gamma(1-\mathcal{E}')]$.

Appendix C. Relaxation to thermal equilibrium of a photon gas: Kompaneets equation

We recall the main steps in the derivation of (4.3), see Kompaneets (1957). In the Thomson limit $\hbar\omega \ll mc^2$, the energy exchange of one transition is small compared with the energy of the photon $\delta\omega = |\omega' - \omega| \ll \omega$. The energy exchange over one Compton event is

$$\hbar\delta\omega = \hbar\omega\frac{c\boldsymbol{p}\cdot\left(\hat{\boldsymbol{k}}' - \hat{\boldsymbol{k}}\right) - \hbar\omega\left(1 - \hat{\boldsymbol{k}}'\cdot\hat{\boldsymbol{k}}\right)}{\gamma mc^2 + \hbar\omega\left(1 - \hat{\boldsymbol{k}}'\cdot\hat{\boldsymbol{k}}\right) - c\boldsymbol{p}\cdot\hat{\boldsymbol{k}}} \tag{C 1}$$

$$\simeq \hbar\omega\left[\frac{\boldsymbol{p}}{mc}\cdot\left(\hat{\boldsymbol{k}}' - \hat{\boldsymbol{k}}\right) - \frac{\hbar\omega}{mc^2}\left(1 - \hat{\boldsymbol{k}}'\cdot\hat{\boldsymbol{k}}\right)\right], \tag{C 2}$$

where $\hat{\boldsymbol{k}} = \boldsymbol{k}/k$ and $\hat{\boldsymbol{k}}' = \boldsymbol{k}'/k'$ are the unit vectors that identify the photon propagation direction before and after scattering. In such regime, the functions f'_e and n' can be expanded to second order in the small parameter $\delta\omega$ allowing the reduction of the full

https://doi.org/10.1017/S002237782000118X Published online by Cambridge University Press

collision operator (4.2) to a Fokker–Planck equation

$$\frac{\partial n}{c\partial t} \simeq \left[\frac{\partial n}{\partial \xi} + n(1+n)\right] \int \mathrm{d}\boldsymbol{p} \frac{\mathrm{d}\sigma}{\mathrm{d}\Omega} f_e \frac{\hbar \delta\omega}{k_B T} + \left[\frac{\partial^2 n}{\partial \xi^2} + (1+n)\left(2\frac{\partial n}{\partial \xi} + n\right)\right] \int \mathrm{d}\boldsymbol{p} \frac{\mathrm{d}\sigma}{\mathrm{d}\Omega} f_e \left(\frac{\hbar \delta\omega}{k_B T}\right)^2, \tag{C 3}$$

where the electron distribution function is assumed to be Maxwellian, and $\xi = \hbar\omega/k_B T$ is the energy of the photon normalised to the electron temperature. The expansion parameter $\delta\omega$ is small in the laboratory frame only if it is also small in the proper frame of each electron. This holds for non-relativistic electron temperatures $k_B T \ll mc^2$. The two integrals in $\delta\omega$ and in $\delta\omega^2$ can be evaluated assuming the differential cross section in the Thomson limit

$$\frac{\mathrm{d}\sigma}{\mathrm{d}\Omega} = \frac{r_e^2}{2}\left(1 + \cos^2\theta\right). \tag{C 4}$$

Then, the time evolution of the average occupation photon number n reads

$$\xi^2 \frac{\partial n}{\partial y} = \frac{\partial}{\partial \xi}\left[\xi^4 \left(\frac{\partial n}{\partial \xi} + n + n^2\right)\right], \tag{C 5}$$

where $y = t/t_C$ is the time normalised to $t_C = mc/\sigma_T n_e k_B T$ and n_e is the electron gas density. The time t_C is the characteristic relaxation time of the process and the thermal equilibrium is reached when $y > 1$.

In regimes where the photon occupation number is small, $n \ll 1$, the photon electron gas interaction is mediated by single Compton scattering events and the equation reduces to its linear form

$$\xi^2 \frac{\partial n}{\partial y} = \frac{\partial}{\partial \xi}\left[\xi^4 \left(\frac{\partial n}{\partial \xi} + n\right)\right]. \tag{C 6}$$

In terms of the photon energy distribution function $f = \xi^2 n$, the linear Kompaneets equation reads

$$\frac{\partial f}{\partial y} = \frac{\partial}{\partial \xi}\left[\xi^2 \frac{\partial f}{\partial \xi} + \left(\xi^2 - 2\xi\right) f\right]. \tag{C 7}$$

REFERENCES

Abe, T. 1993 Generalized scheme of the no-time-counter scheme for the DSMC in rarefied gas flow analysis. *Comput. Fluids* **22** (2), 253–257.

Bird, G. A. 1989 Perception of numerical methods in rarefied gasdynamics. *Prog. Astronaut. Aeronaut.* **117**, 211–226.

Birdsall, C. K. & Langdon, A. B. 1991 *Plasma Physics via Computer Simulation*. Taylor & Francis.

Blackburn, T. G., Ridgers, C. P., Kirk, J. G. & Bell, A. R. 2014 Quantum radiation reaction in laser–electron-beam collisions. *Phys. Rev. Lett.* **112**, 015001.

Blumenthal, G. R. & Gould, R. J. 1970 Bremsstrahlung, synchrotron radiation, and Compton scattering of high-energy electrons traversing dilute gases. *Rev. Mod. Phys.* **42**, 237–270.

Compton, A. H. 1923 A quantum theory of the scattering of x-rays by light elements. *Phys. Rev.* **21**, 483–502.

Dawson, J. M. 1983 Particle simulation of plasmas. *Rev. Mod. Phys.* **55**, 403–447.

Del Gaudio, F., Fonseca, R. A., Silva, L. O. & Grismayer, T. 2020 Plasma wakes driven by photon bursts via Compton scattering. *Phys. Rev. Lett.* arXiv:2003.04249v2.

https://doi.org/10.1017/S002237782000118X Published online by Cambridge University Press

DREICER, H. 1964 Kinetic theory of an electron-photon gas. *Phys. Fluids* **7**, 735.

EVANS, M. W. & HARLOW, F. H. 1957 The particle-in-cell method for hydrodynamic calculations. Los Alamos Scientific Laboratory report LA-2139.

FREDERIKSEN, J. T., HAUGBØLLE, T. & NORDLUND, Å. 2008 Trans-debye scale plasma modeling & stochastic GRB wakefield plasma processes. *AIP Conf. Proc*. **1054** (1), 87–97.

GONOSKOV, A., BASTRAKOV, S., EFIMENKO, E., ILDERTON, A., MARKLUND, M., MEYEROV, I., MURAVIEV, A., SERGEEV, A., SURMIN, I. & WALLIN, E. 2015 Extended particle-in-cell schemes for physics in ultrastrong laser fields: review and developments. *Phys. Rev.* E **92**, 023305.

GOUDSMIT, S. & SAUNDERSON, J. L. 1940 Multiple scattering of electrons. *Phys. Rev*. **57**, 24–29.

GRISMAYER, T., VRANIC, M., MARTINS, J. L., FONSECA, R. A. & SILVA, L. O. 2016 Laser absorption via quantum electrodynamics cascades in counter propagating laser pulses. *Phys. Plasmas* **23** (5), 056706.

GRISMAYER, T., VRANIC, M., MARTINS, J. L., FONSECA, R. A. & SILVA, L. O. 2017 Seeded qed cascades in counterpropagating laser pulses. *Phys. Rev.* E **95**, 023210.

GROOT, S. R., LEEUWEN, W. A. & VAN WEERT, C. G. 1980 *Relativistic Kinetic Theory: Principles and Applications*. North Holland Publishing Company.

HAUGBØLLE, T. 2005 Modelling relativistic astrophysics at the large and small scale. arXiv:astro-ph/0510292.

HAUGBØLLE, T., FREDERIKSEN, J. T. & NORDLUND, Å. 2013 Photon-plasma: a modern high-order particle-in-cell code. *Phys. Plasmas* **20** (6), 062904.

HIGGINSON, D. P. 2017 A full-angle Monte-Carlo scattering technique including cumulative and single-event Rutherford scattering in plasmas. *J. Comput. Phys*. **349**, 589–603.

HOCKNEY, R. W. & EASTWOOD, J. W. 1988 *Computer Simulation Using Particles*. CRC Press.

JACKSON, J. D. 1999 *Classical Electrodynamics*, 3rd ed. John Wiley & Sons.

JIRKA, M., KLIMO, O., BULANOV, S. V., ESIRKEPOV, T. Z., GELFER, E., BULANOV, S. S., WEBER, S. & KORN, G. 2016 Electron dynamics and γ and $e^{-}e^{+}$ production by colliding laser pulses. *Phys. Rev.* E **93**, 023207.

KAWAMURA, E. & BIRDSALL, C. K. 2005 Effect of coulomb scattering on low-pressure high-density electronegative discharges. *Phys. Rev.* E **71**, 026403.

KLEIN, O. & NISHINA, Y. 1923 The scattering of light by free electrons according to Dirac's new relativistic dynamics. *Nature* **122**, 398–399.

KOMPANEETS, A. S. 1957 The establishment of thermal equilibrium between quanta and electrons. *Sov. Phys. JETP* **4**, 730.

LANDAU, L. D. & LIFSHITZ, E. M. 1975 *The Classical Theory of Fields*. Pergamon Press plc.

LARSON, D. J. 2003 A Coulomb collision model for PIC plasma simulation. *J. Comput. Phys*. **188** (1), 123–138.

LOBET, M., D'HUMIÉRES, E., GRECH, M., RUYER, C., DAVOINE, X. & GREMILLET, L. 2016 Modeling of radiative and quantum electrodynamics effects in PIC simulations of ultra-relativistic laser-plasma interaction. *J. Phys.: Conf. Ser*. **688**, 012058.

MILLER, R. H. & COMBI, M. R. 1994 A coulomb collision algorithm for weighted particle simulations. *Geophys. Res. Lett*. **21** (16), 1735–1738.

NANBU, K. 1997 Theory of cumulative small-angle collisions in plasmas. *Phys. Rev.* E **55**, 4642–4652.

NERUSH, E. N., KOSTYUKOV, I. Y., FEDOTOV, A. M., NAROZHNY, N. B., ELKINA, N. V. & RUHL, H. 2011 Laser field absorption in self-generated electron-positron pair plasma. *Phys. Rev. Lett*. **106**, 035001.

PEANO, F., MARTI, M., SILVA, L. O. & COPPA, G. 2009 Statistical kinetic treatment of relativistic binary collisions. *Phys. Rev.* E **79**, 025701.

PEYRAUD, J. 1968*a* Théorie cinétique des plasmas, interaction matiére-rayonnement: I. *J. Phys*. **29**, 88.

PEYRAUD, J. 1968*b* Théorie cinétique des plasmas, interaction matiére-rayonnement: II. *J. Phys*. **29**, 306.

PEYRAUD, J. 1968*c* Théorie cinétique des plasmas, interaction matiére-rayonnement: III. *J. Phys*. **29**, 872.

RIDGERS, C. P., BRADY, C. S., DUCLOUS, R., KIRK, J. G., BENNETT, K., ARBER, T. D., ROBINSON, A. P. L. & BELL, A. R. 2012 Dense electron-positron plasmas and ultraintense γ rays from laser-irradiated solids. *Phys. Rev. Lett*. **108**, 165006.

https://doi.org/10.1017/S002237782000118X Published online by Cambridge University Press

SENTOKU, Y. & KEMP, A. J. 2008 Numerical methods for particle simulations at extreme densities and temperatures: weighted particles, relativistic collisions and reduced currents. *J. Comput. Phys*. **227** (14), 6846–6861.

SHERLOCK, M. 2008 A Monte-Carlo method for coulomb collisions in hybrid plasma models. *J. Comput. Phys*. **227** (4), 2286–2292.

SUNYAEV, R. A. & ZEL'DOVICH, Y. B. 1980 Microwave background radiation as a probe of the contemporary structure and history of the universe. *Annu. Rev. Astron. Astrophys*. **18**, 537.

TAKIZUKA, T. & ABE, H. 1977 A binary collision model for plasma simulation with a particle code. *J. Comput. Phys*. **25** (3), 205–219.

THOMSON, J. J. 1906 *Conduction of Electricity through Gases*. University Press.

TURRELL, A. E., SHERLOCK, M. & ROSE, S. J. 2015 Self-consistent inclusion of classical large-angle coulomb collisions in plasma Monte Carlo simulations. *J. Comput. Phys*. **299**, 144–155.

VAHEDI, V. & SURENDRA, M. 1995 A Monte Carlo collision model for the particle-in-cell method: applications to argon and oxygen discharges. *Comput. Phys. Commun*. **87** (1), 179–198.

VRANIC, M., GRISMAYER, T., FONSECA, R. A. & SILVA, L. O. 2016*a* Electron–positron cascades in multiple-laser optical traps. *Plasma Phys. Control. Fusion* **59** (1), 014040.

VRANIC, M., GRISMAYER, T., FONSECA, R. A. & SILVA, L. O. 2016*b* Quantum radiation reaction in head-on laser-electron beam interaction. *New J. Phys*. **18** (7), 073035.

VRANIC, M., GRISMAYER, T., MARTINS, J. L., FONSECA, R. A. & SILVA, L. O. 2015 Particle merging algorithm for PIC codes. *Comput. Phys. Commun*. **191**, 65–73.

VRANIC, M., MARTINS, J. L., VIEIRA, J., FONSECA, R. A. & SILVA, L. O. 2014 All-optical radiation reaction at 10^{21} W/cm^2. *Phys. Rev. Lett*. **113**, 134801.

WILSON, G. R., HORWITZ, J. L. & LIN, J. 1992 A semikinetic model for early stage plasmasphere refilling: 1, effects of coulomb collisions. *J. Geophys. Res*. **97** (A2), 1109–1119.